ADVANCED FUNCTIONAL MATERIALS
www.afm-journal.de

Magnesium Ions Direct the Solid-State Transformation of Amorphous Calcium Carbonate Thin Films to Aragonite, Magnesium-Calcite, or Dolomite

*Shuheng Zhang, Ouassef Nahi, Li Chen, Zabeada Aslam, Nikil Kapur, Yi-Yeoun Kim, and Fiona C. Meldrum**

Amorphous calcium carbonate (ACC) is a common precursor to crystalline calcium carbonate, and is of particular importance in biomineralization, where its crystallization in privileged environments ensures a pseudomorphic transformation. While organisms regulate this process using organic molecules and magnesium ions to selectively form calcite or aragonite, it has proven highly challenging to replicate this polymorph selectivity synthetically. Here, it is demonstrated that remarkable control can be achieved over the chemical composition and structure of crystalline calcium carbonate by using heat to drive a pseudomorphic transformation of ACC thin films. The crystal polymorph can be tuned from low magnesium-calcite to pure aragonite, high magnesium-calcite, and ultimately dolomite according to the magnesium content of the ACC, and mosaics of large single crystals are generated at elevated temperatures rather than the spherulitic structures formed at room temperature. This methodology also enables an in situ investigation of the ACC crystallization mechanism using transmission electron microscopy. Finally, the approach can be combined with templating methods to generate arrays of large aragonite single crystals with preselected morphologies. These results demonstrate that exceptional control can be achieved through the solid-state transformation of Mg-ACC, which has relevance to both synthetic and biological systems.

1. Introduction

Biomineralization processes demonstrate that it is possible to achieve exceptional control over crystallization. This is well-illustrated by the calcium carbonate system, in which organisms select the polymorph with perfect fidelity, tune the structure from single crystals to polycrystalline materials, generate complex morphologies and control orientation. Organisms can achieve such high levels of control by stabilizing, and then controlling the crystallization of an amorphous calcium carbonate (ACC) precursor phase.[1–3] Crucially, ACC is contained in a privileged environment deprived of bulk water[4] such that crystallization occurs via a pseudomorphic transformation[5] rather than a dissolution/reprecipitation mechanism that commonly takes place in bulk solution.[6] Organisms can also determine where and when nucleation occurs, and can mold the product crystal morphology by templating the amorphous precursor. Biogenic ACC also contains magnesium ions and organic molecules that extend its lifetime and play a critical role in determining the polymorph of the product crystal.[7,8]

However, while ACC widely transforms to both calcite[2,4] and aragonite[9,10] during biomineralization, very few examples exist of the transformation of ACC to aragonite in synthetic aqueous systems.[11–13] Similarly, the pseudomorphic transformation of ACC containing magnesium ions (Mg-ACC) to single crystals of high magnesium calcite occurs in many organisms, but there are few comparable examples in synthetic systems.[14,15] Magnesium ions are ubiquitous in biology and the environment,[16,17] and both extend the lifetime of ACC and alter the morphologies of calcite crystals.[6,18–20] They also change the composition and physical properties of calcite through their incorporation in the crystal lattice.[21] Low magnesium calcites form readily,[14] but the precipitation of high

S. Zhang, O. Nahi, Y.-Y. Kim, F. C. Meldrum
School of Chemistry
University of Leeds
Woodhouse Lane, Leeds LS2 9JT, UK
E-mail: F.Meldrum@leeds.ac.uk

The ORCID identification number(s) for the author(s) of this article can be found under https://doi.org/10.1002/adfm.202201394.

DOI: 10.1002/adfm.202201394

L. Chen
School of Electronic and Electrical Engineering
University of Leeds
Woodhouse Lane, Leeds LS2 9JT, UK

Z. Aslam
School of Chemical and Process Engineering
University of Leeds
Woodhouse Lane, Leeds LS2 9JT, UK

N. Kapur
School of Mechanical Engineering
University of Leeds
Woodhouse Lane, Leeds LS2 9JT, UK

magnesium calcites from solution is challenging, and they are typically polycrystalline.[18,22–24] Yet organisms such as echinoderms generate large skeletal elements that diffract as single crystals with average Mg contents > 10 mol% Mg.[15] Notably, magnesium ions can also promote aragonite formation, where it is difficult to produce this metastable phase at room temperature in aqueous solutions in their absence.[23,25–27]

Here, we study the solid-state transformation of ACC thin films prepared in the presence of magnesium ions and poly (acrylic acid) (PAA), using heat to control nucleation and growth, and to ensure that transformation occurs with retention of morphology. The results show that the structure, composition, and polymorph of the product crystalline films can be controlled according to the chemical composition of the ACC precursor and the heating regime applied. While films produced at room temperature have spherulitic structures, mild-isothermal heating generated a mosaic of tabular single crystals up to several hundreds of micrometers in size. Importantly, the crystal structure of the annealed films can be controlled according to the magnesium content of the ACC precursor, and pure aragonite films comprising single crystal domains are formed at very low magnesium concentrations. With the ability to characterize the thin films using transmission electron microscopy (TEM), these experiments complement studies of magnesium ACC using thermal analysis techniques such as thermogravimetric analysis (TGA),[19,28,29] where these provide information on the energetics of the crystallization, but not on the structure of the products.

2. Results

2.1. Preparation of ACC Thin Films

ACC thin films were prepared using the ammonia diffusion method (ADM)[30] in the presence of Mg^{2+} ions and small amounts of PAA. PAA induces the formation of an amorphous polymer-induced liquid precursor (PILP) phase that readily forms uniform ACC films,[5] while Mg^{2+} ions have a potent effect on calcium carbonate precipitation, and retard crystallization.[6,18,19] Precipitation reactions were carried out within small volumes (≈50 µL) of 10×10^{-3} M $CaCl_2$ solutions containing 0–100×10^{-3} M Mg^{2+} ions and 0–20 µg mL^{-1} PAA (Table S1, Supporting Information), where silicon wafers or TEM grids were placed at the base of the reaction wells (**Figure 1**A). Uniform and continuous films formed in the presence of PAA and Mg^{2+}, and polarized optical microscopy (POM), bright field TEM and associated selected area electron diffraction (SAED) confirmed their amorphous structures (Figure 1B–D). The film thickness was estimated as ≈100 nm using atomic force microscopy (AFM) (Figure S1, Supporting Information). Notably, continuous films did not form in the absence of Mg^{2+} ions and PAA, where Mg^{2+} ions increase the wettability of the PILP phase, leading to the formation of a continuous ACC film.[31]

2.2. Composition of ACC Thin Films

The magnesium contents of the ACC films were determined using inductively coupled plasma-optical emission spectrometry (ICP-OES) after dissolution in dilute HCl solution. Values were determined as an average of at least 10 samples, and were consistent with levels determined using energy dispersive X-ray (EDX) analysis. The magnesium contents of the ACC films scaled with the concentrations of the Mg^{2+} ions and PAA in the reaction solution (**Table 1**). Films produced in the presence of Mg^{2+} ions alone had very low magnesium contents at $[Mg^{2+}] = 4 \times 10^{-3}$ M, as compared with 5.3 mol% at $[Mg^{2+}] = 10 \times 10^{-3}$ M, 21.6 mol% at $[Mg^{2+}] = 50 \times 10^{-3}$ M, and 42.2 mol% at $[Mg^{2+}] = 100 \times 10^{-3}$ M. This is consistent with reports of the precipitation of Mg-ACC in aqueous solution which have shown that Mg^{2+} ions incorporate within ACC at levels that reflect both the Ca/Mg ratio in solution and the rate of precipitation.[32,33] PAA enhances the magnesium content of the ACC, as evidenced by an increase in the Mg content from 5.3 to 10.1 mol% on raising PAA from 0 to 8 µg mL^{-1} at constant $[Mg^{2+}] = 10 \times 10^{-3}$ M. This effect was more pronounced at low concentrations of Mg, and can be attributed to the stronger complexation of PAA molecules with calcium than magnesium ions, such that the ratio of available Mg/Ca in the reaction solution is increased.[34]

2.3. Crystallization of ACC Films under Ambient Conditions

ACC films prepared with $[Mg^{2+}] < 30 \times 10^{-3}$ M crystallized within 3 days under ambient conditions to give continuous crystalline films comprising mosaics of spherulitic domains of sizes ≈200–500 µm (Figure 1E). The compositions of the ACC films had a significant influence on the induction times, where both Mg^{2+} ions and PAA delay the onset of crystallization. For example, films prepared with $[Mg^{2+}] = 10 \times 10^{-3}$ M and [PAA] = 2 µg mL^{-1} crystallized within 18 h, while those prepared with $[Mg^{2+}] = 20 \times 10^{-3}$ M and [PAA] = 2 µg mL^{-1} took 3 days to crystallize. Extremely stable ACC films that remained amorphous for over 30 days were formed at high magnesium concentrations of $[Mg^{2+}] = 50$–100×10^{-3} M.

The structures of the crystalline films were determined using TEM and SAED. The vast majority of samples were polycrystalline calcite (Figure 1E–G), but those prepared at $[Mg^{2+}] = 2$–4×10^{-3} M and [PAA] = 0–2 µg mL^{-1} also contained some domains of polycrystalline aragonite (Figure 1H–K). These results are consistent with previous observations of the crystallization of ACC thin films under ambient conditions, although pseudomorphic transformation of ACC to aragonite at room temperature is rare. At room temperature, magnesium-free ACC films typically transform into polycrystalline calcite or vaterite with spherulitic and/or mosaic-type structures.[35,36] The addition of Mg^{2+} ions increases the proportion of spherulitic domains, and thin films comprising single crystal domains of magnesium calcite and aragonite were generated under Langmuir monolayers based on resorcarene.[11]

2.4. Crystallization of ACC Films Using Heat Treatment

Controlled crystallization of the amorphous thin films was achieved using heat treatment, where this provides an effective means of directing the structure and polymorph of the product

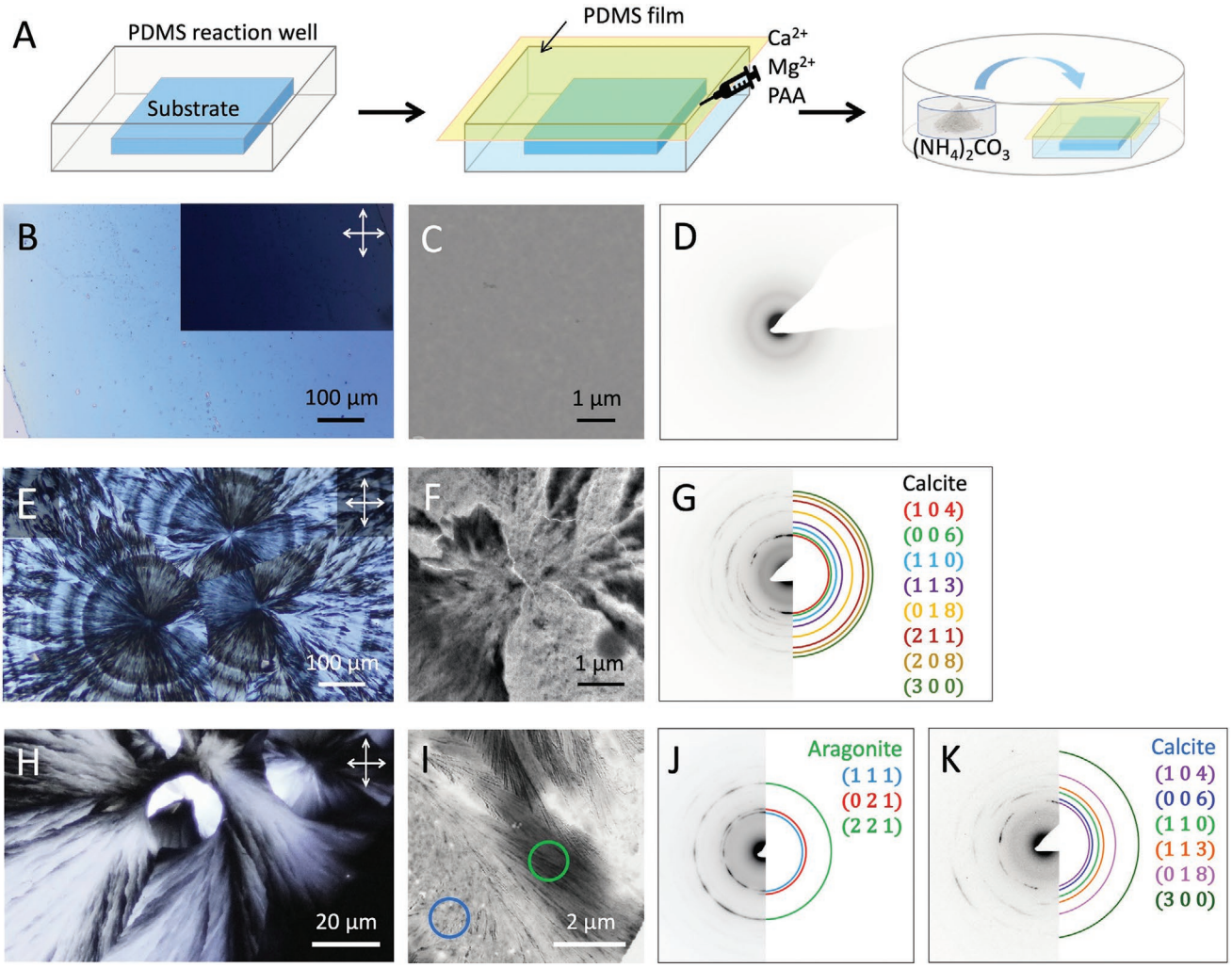

Figure 1. Preparation of ACC films and their crystallization under ambient conditions. A) Schematic illustration of the deposition process of the ACC films. A silicon substrate was placed at the base of a 1 mm deep PDMS reaction well. The PDMS well was covered by a gas-permeable PDMS film and filled with the precipitation solution using a syringe and the cell was placed in a sealed Petri dish containing $(NH_4)_2CO_3$ powder to initiate ACC precipitation. B–D) ACC films prepared at $[Ca^{2+}] = 10 \times 10^{-3}$ M, $[Mg^{2+}] = 20 \times 10^{-3}$ M, and [PAA] = 2 µg mL^{-1}, as characterized by B) OM and POM (inset), C) bright-field TEM and D) SAED. E–G) Calcite films with spherulitic structures prepared under the same solution conditions as B) and crystallized under ambient conditions for 2 days, as characterized by E) POM, F) bright-field TEM, and G) SAED. H–K) Spherulitic films comprising calcite and aragonite prepared at $[Ca^{2+}] = 10 \times 10^{-3}$ M, $[Mg^{2+}] = 2 \times 10^{-3}$ M, and [PAA] = 2 µg mL^{-1}, and crystallized under ambient conditions for 2 days. The corresponding films were characterized by H) POM, I) bright-field TEM, and J,K) SAED, where J) corresponds to aragonite denoted by green circle in I), and K) corresponds to calcite denoted by the blue circle in I).

crystalline film. Thin films were placed on a heating stage and the temperature was increased by 10 °C min^{-1} (equivalent to typical TGA measurements). In situ POM was used to identify the temperature at which crystallization was initiated—the onset nucleation temperature (T_{ON})—and the film was then incubated at T_{ON} until crystallization was completed. This typically occurred within 5 h for a millimeter-sized film, and all of the films comprised mosaics of single crystal domains (**Figure 2**). If the heat ramp is continued rather than incubating the sample at T_{ON}, polycrystallinity develops at the growth front and the entire film ultimately becomes polycrystalline in structure (Figure S2, Supporting Information).

T_{ON} directly correlated with the magnesium content of the ACC film, where those prepared at $[Mg^{2+}] = 10 \times 10^{-3}$ M and [PAA] = 2 µg mL^{-1} crystallized at T_{ON} = 150 °C, as compared with T_{ON} = 260 °C for films prepared at $[Mg^{2+}] = 20 \times 10^{-3}$ M and [PAA] = 2 µg mL^{-1}. Crystallization temperatures as high as 350 ± 50 °C were recorded for films prepared at $[Mg^{2+}] = 75 \times 10^{-3}$ M and [PAA] = 2 µg mL^{-1}. All of the product thin films comprised a mosaic of single crystals, whose sizes were governed by the magnesium content of the precursor ACC films. These varied from 100 to 500 µm for low magnesium ACC films prepared at $[Mg^{2+}] = 10 \times 10^{-3}$ M, to 50–100 µm for those prepared at $[Mg^{2+}] = 20 \times 10^{-3}$ M, and 10–50 µm at $[Mg^{2+}] = 75 \times 10^{-3}$ M (Figure 2). The heated films therefore always exhibited smaller single-crystal domains than their spherulitic counterparts formed under ambient conditions, due to the increase in nucleation rate with temperature.

Table 1. Summary of the Mg^{2+} ions content of ACC films and the product crystalline films produced under annealing using various precipitation conditions. The Mg-content of the ACC films was estimated using ICP-OES and that of the crystalline films using EDX. The limit of detection (LOD) of ICP-OES was 0.57 mol% Mg. The polymorph of the product crystalline films was determined by TEM.

$[Ca^{2+}]$ [$\times 10^{-3}$ M]	$[Mg^{2+}]$ [$\times 10^{-3}$ M]	[PAA] [μg mL^{-1}]	Mg in ACC films [mol%]	Mg in crystalline $CaCO_3$ films [mol%]	Phases obtained upon heating
10	0	2	< LOD	0	Calcite
10	0	4	< LOD	0	Calcite
10	0	20	< LOD	0	Calcite
10	2	0	< LOD	0.2 ± 0.1	Aragonite
10	4	0	< LOD	1.0 ± 0.3	Aragonite
10	2	2	1.45 ± 0.05	1.5 ± 0.5	Aragonite and calcite
10	4	4	5.28 ± 0.16	5.7 ± 1.2	Low Mg-calcite with 2–10 mol% Mg
10	10	0	5.28 ± 0.16	6.1 ± 1.4	
10	10	2	7.78 ± 0.23	7.5 ± 1.6	
10	10	4	9.94 ± 0.29	9.3 ± 2.1	
10	10	8	10.09 ± 0.29	10.9 ± 2.3	High Mg-calcite with 10–50 mol% Mg
10	15	2	11.43 ± 0.32	11.3 ± 2.4	
10	15	4	12.60 ± 0.35	12.2 ± 2.7	
10	20	2	17.61 ± 0.46	16.7 ± 3.6	
10	50	0	21.62 ± 0.54	25.5 ± 4.3	
10	75	0	29.69 ± 0.67	29.5 ± 5.3	
10	75	2	33.07 ± 0.71	32.2 ± 5.5	
10	100	0	42.21 ± 0.75	49.3 ± 14.3	Dolomite

The magnesium contents of the crystalline films were estimated using scanning transmission electron microscopy (STEM-EDX). All ACC films containing 5–32 mol% Mg^{2+} ions transformed to Mg-calcite and excellent correlation was observed between the Mg-contents of the precursor ACC films and the product calcite single crystals (Table 1). Mg levels of between 6 and 11 mol% were achieved at a Ca/Mg molar ratio of 1 as the PAA concentration was increased from 0 to 8 μg mL^{-1}, while contents as high as 32 mol% were achieved at Ca/Mg = 10/75 and [PAA] = 2 μg mL^{-1}. An approximately linear correlation was observed between the Mg content of the crystalline films and the Mg/Ca ratio in the reaction solution, and the presence of PAA increased the Mg content (Figure S3, Supporting Information). EDX mapping across the interface in a partially crystallized sample further confirmed that the Mg concentration was equivalent in both the precursor Mg-ACC and product magnesian calcite phases (**Figure 3**).

TEM and SAED also provided information about the structures of the Mg-calcite films. Recent studies of calcite optical lenses found in the brittlestar *Ophiocoma wendtii* containing 15 mol% Mg showed that although they diffract as single crystals, they actually comprise high-Mg nanoparticles embedded in a low Mg-calcite matrix.[15] A coherent interface exists between these two phases. This structure has been proposed to arise from a spinodal decomposition of the precursor Mg-ACC phase.[37] No evidence for two phases was found in bright field TEM images of any of the high magnesium calcite crystals generated in our study. Volume changes during crystallization are minimal for ACC films prepared at low magnesium concentrations (with 2–10 mol% Mg). This is shown by the absence of film cracking or shrinking in the TEM images of the crystallization process (Figure 2A). In contrast, ACC films containing higher magnesium (10–18 mol% Mg) do crack after annealing, showing that stresses occur in these films due to a volume shrinkage associated with dehydration (Figure S4, Supporting Information). The single crystal domains in high Mg-calcite also often showed fuzzy bend contours that are indicative of high tensile stresses (Figure 2C).[38]

Further confirmation that the Mg was present as a uniform solid solution in the calcite lattice was obtained by characterizing the single crystal calcite domains using high-resolution TEM (HRTEM) (**Figure 3**A). The calcite lattice shrinks on doping with the smaller Mg^{2+} ions,[18] such that the Mg content of the calcite crystals can be estimated based on the measured lattice spacing (Figure S5, Supporting Information). The small quantities of occluded polymer have a negligible effect on the lattice parameters.[39,40] Good agreement is again found between the Mg-content of the calcite films as estimated using EDX and HRTEM (Table S2, Supporting Information), which further demonstrates the uniform structure of the Mg-calcite.

ACC with yet higher Mg contents of 42 mol% were formed at $[Mg^{2+}] = 100 \times 10^{-3}$ M and [PAA] = 0 μg mL^{-1}. These films crystallized at high temperatures with T_{ON} of 450 ± 50 °C, where they transformed to a mosaic of single crystals of ordered dolomite with domain sizes of 5–10 μm. Dolomite was confirmed by the presence of (101) reflections in SAED (**Figure 4**),[41] and HRTEM lattice images showed {104} spacings of 2.91 Å, as compared with 2.90 Å in geological dolomite.[42] STEM-EDX confirmed equivalent Mg contents in the dolomite films as in the precursor ACC films (Figure S6, Supporting Information).

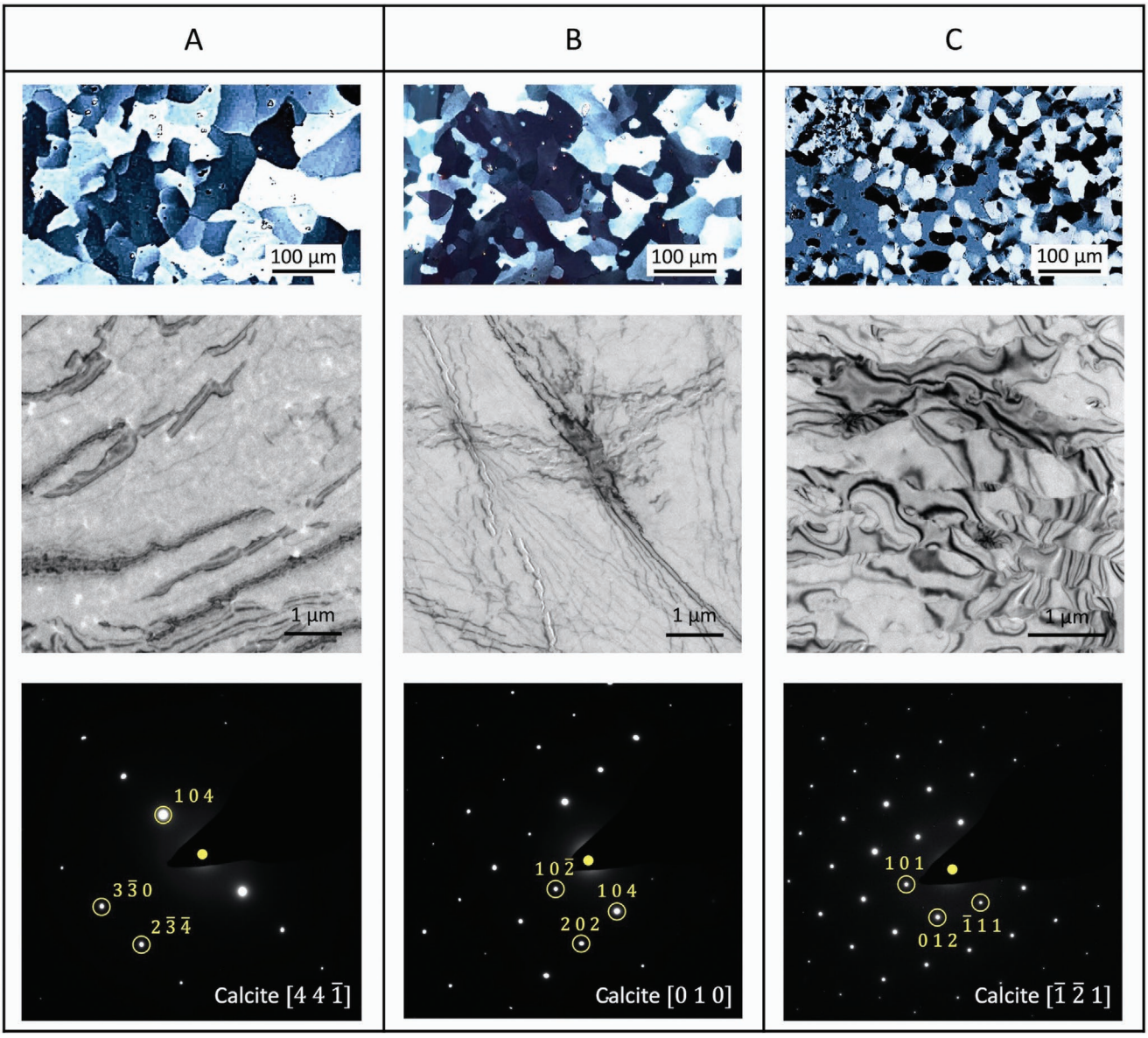

Figure 2. A–C) POM, bright-field TEM images and corresponding SAED patterns of three calcite films prepared by incubating the ACC films in an oven for 5 h. A) ACC films prepared from solutions comprising $[Mg^{2+}] = 10 \times 10^{-3}$ M and [PAA] = 2 µg mL^{-1}, and crystallized at 150 °C for 5 h. B) ACC films precipitated from solutions comprising $[Mg^{2+}] = 20 \times 10^{-3}$ M and [PAA] = 2 µg mL^{-1}, and crystallized at 260 °C for 5 h. C) ACC films prepared from solutions comprising $[Mg^{2+}] = 75 \times 10^{-3}$ M and [PAA] = 2 µg mL^{-1}, crystallized at 350 °C for 5 h.

2.5. Control over Crystal Polymorph—Aragonite Single Crystals

Screening ACC films with a wide range of compositions also revealed a fascinating phenomenon—ACC containing small amounts of Mg transformed to aragonite single crystals rather than calcite (Table 1 and **Figure 5**). There are few previous examples of the transformation of ACC to pure aragonite, where PILP films produced in the absence of magnesium usually transform to calcite or vaterite at room temperature or when heated.[36,43] A rare exception is the formation of thin films comprising single crystal magnesium calcite and aragonite tablets under Langmuir monolayers based on resorcarene.[11] Polycrystalline aragonite particles have also been reported within polymer matrices including poly(vinyl alcohol) (PVA)[13] and chitosan[12] in the presence of PAA.

ACC films prepared at $[Mg^{2+}] = 2 \times 10^{-3}$ M or 4×10^{-3} M in the absence of PAA contained up to 1.45 mol% Mg and transformed to mosaics of 10–30 µm aragonite single crystals on heating at 130 °C for 5 h (Figure 5A–D). Addition of PAA to the reaction solution reduced the proportion of aragonite formed. Films prepared at $[Mg^{2+}] = 4 \times 10^{-3}$ M and [PAA] = 4 µg mL^{-1} transformed to pure Mg-calcite at 130 °C, while those prepared at $[Mg^{2+}] = 2 \times 10^{-3}$ M and [PAA] = 2 µg mL^{-1} comprised aragonite with ≈20 vol% calcite, as estimated from bright field TEM and SAED (Figure 5E–H). The aragonite domains in the latter sample were always larger (10–20 µm) than the calcite

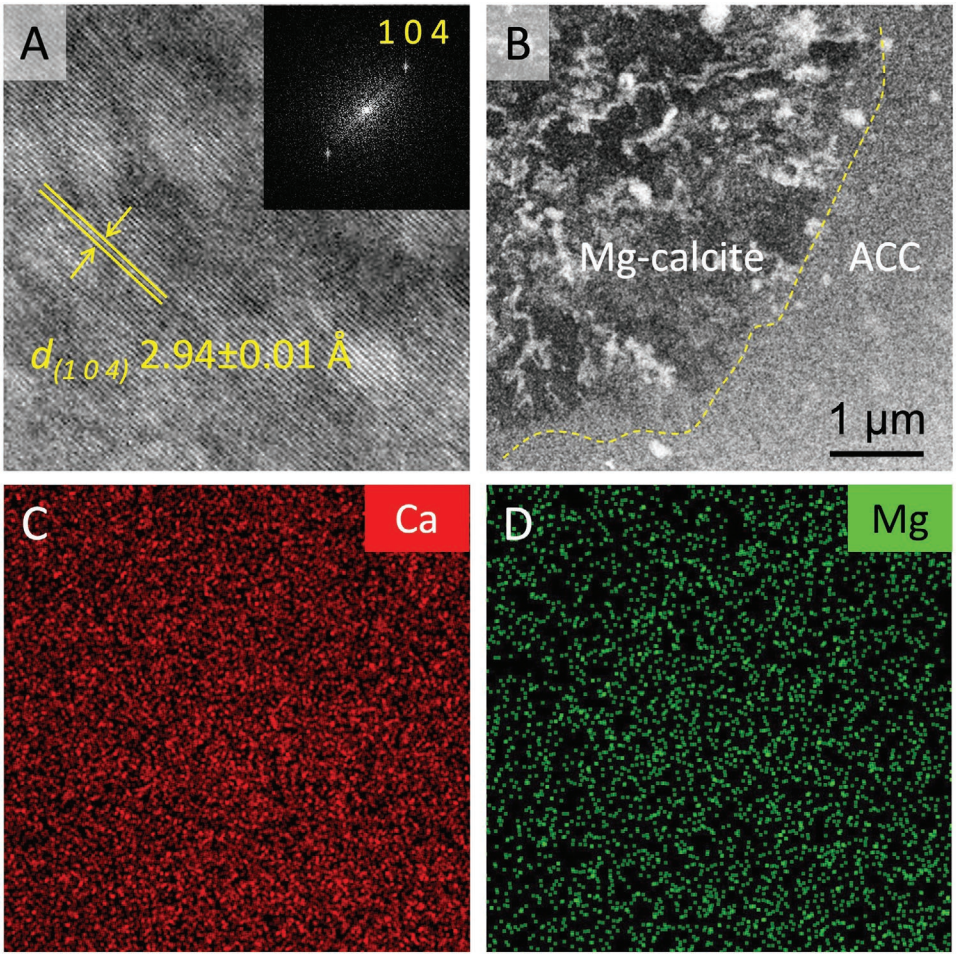

Figure 3. A) HRTEM image of a high Mg-calcite film prepared from solutions comprising $[Ca^{2+}] = 10 \times 10^{-3}$ M, $[Mg^{2+}] = 75 \times 10^{-3}$ M, and [PAA] = 2 μg mL^{-1}, and annealed at 350 °C for 5 h. The inset shows the corresponding FFT diffractogram. B) STEM HAADF image and corresponding EDX maps of the C) Ca and D) Mg at the ACC/calcite boundary in the same sample.

domains (2–5 μm). This indicates that calcite nucleates later than aragonite, as both phases exhibit similar growth rates under these incubation conditions. Crystallization of the same samples under ambient conditions again yielded aragonite, but in reduced amounts and the domains were polycrystalline rather than single crystals. 1:1 vol% calcite/aragonite spherulites formed at room temperature from ACC films prepared at $[Mg^{2+}] = 2 \times 10^{-3}$ M and [PAA] = 2 μg mL^{-1} (Figure 1H–K).

2.6. Patterned Films

The influence of the area of the ACC film on the transformation product was also investigated by patterning the ACC films on the microscale (**Figure 6**), as achieved using standard microfabrication techniques. A template was created by depositing a layer of photoresist on silicon wafers or SiN TEM window grids, and then exposing to UV light through a dark-field mask comprising an array of circles with diameters of 5–20 μm. Immersing the exposed substrates in a bath of developer solution to remove the unexposed photoresist then generates a hydrophobic coating comprising an array of holes on silicon. ACC films were then deposited on these substrates, where this preferentially occurs within the holes on the uncoated silicon. Final lift-off of the remaining photoresist in ethanol then creates an array of ACC disks on the substrate (Figure 6A,B).

Continuous ACC films and ACC disks with diameters of 5 μm were produced under conditions $[Ca^{2+}] = 10 \times 10^{-3}$ M, $[Mg^{2+}] = 2 \times 10^{-3}$ M, and [PAA] = 2 μg mL^{-1} and were incubated at 130 °C for 5 h. Continuous ACC films of the same composition transformed to 4:1 aragonite to calcite under these conditions. The 5 μm diameter ACC domains, in contrast, all transformed to single crystals of aragonite (Figure 6C–E). This behavior demonstrates that there is a fine balance between the energetic barriers to the formation of these phases under these conditions, and suggests that aragonite nucleates first. As less time is required for growth to be completed within a 5 μm domain as compared with a large area, full transformation to a single crystal of aragonite can occur before calcite can nucleate. Transformation to a single crystal is similarly favored within small areas due to the reduction in nucleation probability (Figure S7, Supporting Information).[44]

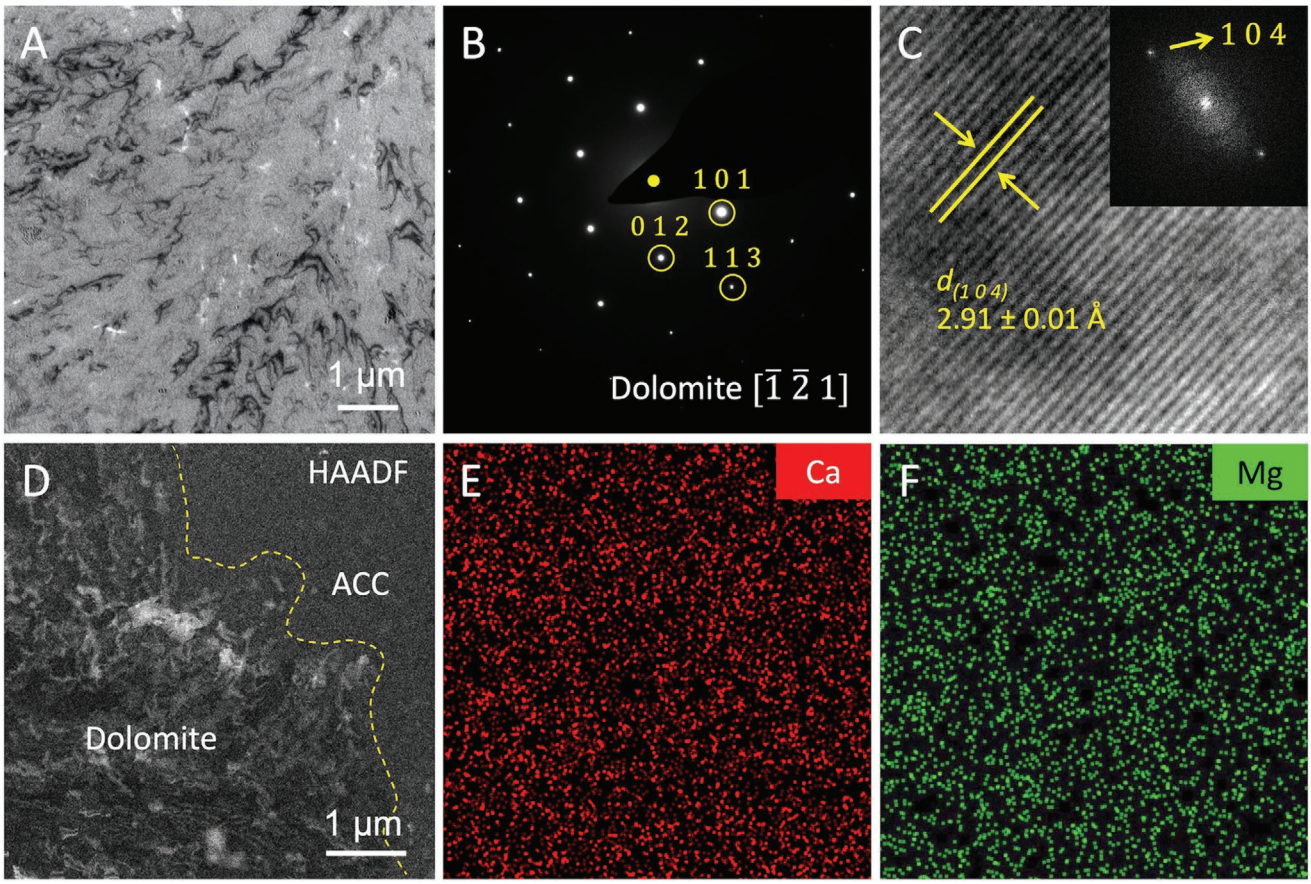

Figure 4. A) Bright-field TEM image and B) corresponding SAED pattern of a single crystal domain in dolomite film generated from ACC films prepared at $[Ca^{2+}] = 10 \times 10^{-3}$ M and $[Mg^{2+}] = 100 \times 10^{-3}$ M and then annealed at 450 °C for 5 h. C) HRTEM image of the dolomite single crystal domain showing {104} lattice fringes with average *d*-spacings of 2.91 ± 0.01 Å. The inset shows the corresponding FFT diffractogram. D) STEM HAADF image and corresponding EDX maps for E) Ca and F) Mg for a partially crystallized area in the same sample. The magnesium ions are uniformly distributed across the amorphous/crystal boundary.

3. Discussion

3.1. Influence of Mg^{2+} Ions on the Crystallization of ACC

Our results show that outstanding control over the structures—and importantly the polymorphs—of calcium carbonate thin films can be achieved by tuning the composition of the ACC precursor and the annealing strategy. Small amounts of PAA promote the formation of continuous ACC films via a PILP process,[5] while Mg^{2+} ions have a pivotal role in stabilizing the ACC and directing the polymorph of the product crystals. Indeed, magnesium ions exert a significant effect on calcium carbonate precipitation from bulk solution, where they delay the nucleation and growth of calcite and can either occlude within the calcite lattice. Significant inhibition results in the formation of aragonite.[16,17] Monohydrocalcite ($CaCO_3.H_2O$) is also commonly formed on transformation of high Mg-ACC in solution,[32] and can again accommodate high levels of magnesium.[45] These effects are usually attributed to the binding of the highly hydrated magnesium ions to the calcite surface,[46] where the Mg^{2+} ions must fully dehydrate prior to their incorporation within the calcite lattice.[17,47] Magnesian calcite is also more soluble than pure calcite, which renders it energetically less stable.[48] Aragonite is little affected by magnesium ions, as they are poorly accommodated within its denser lattice.[16]

The influence of Mg^{2+} ions on the transformation of ACC has been studied extensively.[18,49–52] In solution, Mg-ACC principally crystallizes by a dissolution/reprecipitation mechanism, and calcite formation is impeded by the Mg^{2+} ions released into the solution as the ACC dissolves.[6,29,49,50] Under certain conditions, Mg-ACC has also been observed to transform to calcite with a retention of the original morphology in solutions containing Mg^{2+} ions.[49] This may arise when Mg^{2+} ions in the solution inhibit calcite formation in solution, such that nucleation occurs more readily within the Mg-ACC particles. This did not occur when pure ACC particles were dispersed in a solution of Mg^{2+} ions, suggesting that nucleation was easier within Mg-ACC than pure ACC at room temperature. The reaction conditions and composition of the ACC therefore determine whether nucleation occurs within the ACC or solution.[49] The transformation of ACC under humid conditions, in turn, is mediated by water adsorbed to the ACC, and nucleation occurs due to local dissolution/reprecipitation.[19,53–55] Crystallization then proceeds as the water is expelled from the ACC, where crystallinity propagates from a crystalline to an adjacent amorphous nanoparticle.[53,56]

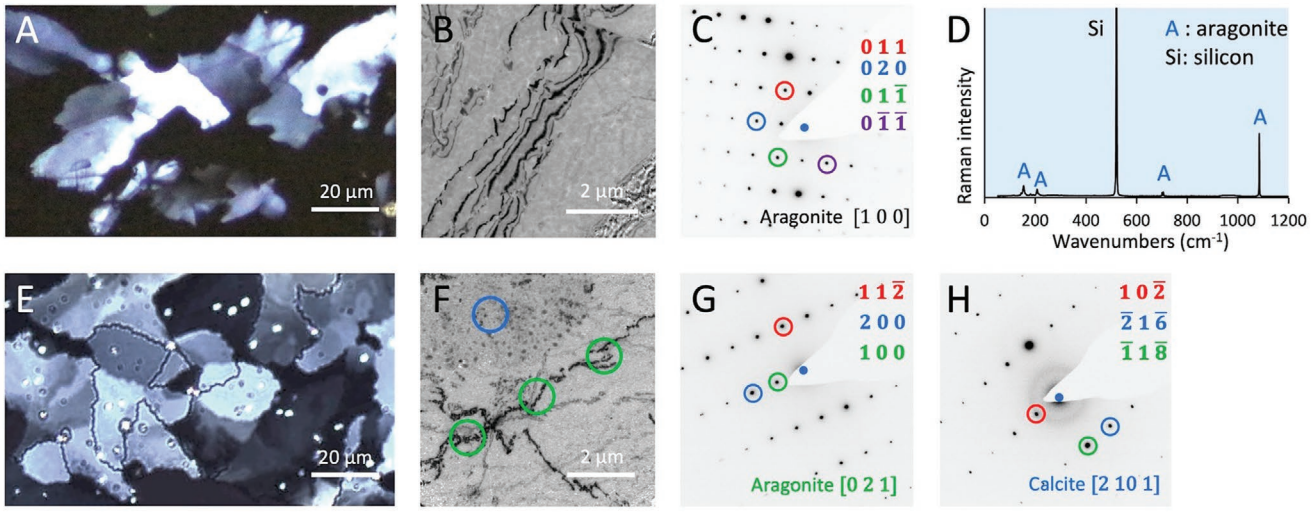

Figure 5. A–D) Aragonite films prepared from solutions comprising $[Ca^{2+}] = 10 \times 10^{-3}$ M and $[Mg^{2+}] = 2 \times 10^{-3}$ M, and heated at 130 °C for 5 h, as characterized by A) POM, B) bright-field TEM, and C) SAED. D) Raman spectroscopy. E–H) Mosaic-like films comprising both calcite and aragonite prepared at $[Ca^{2+}] = 10 \times 10^{-3}$ M, $[Mg^{2+}] = 2 \times 10^{-3}$ M, and [PAA] = 2 µg mL^{-1}, and crystallized by heating at 130 °C for 5 h. The corresponding films are characterized by E) POM, F) bright-field TEM, and G,H) SAED, where G) corresponds to aragonite denoted by the green circles in F), and H) corresponds to calcite denoted by the blue circle in F).

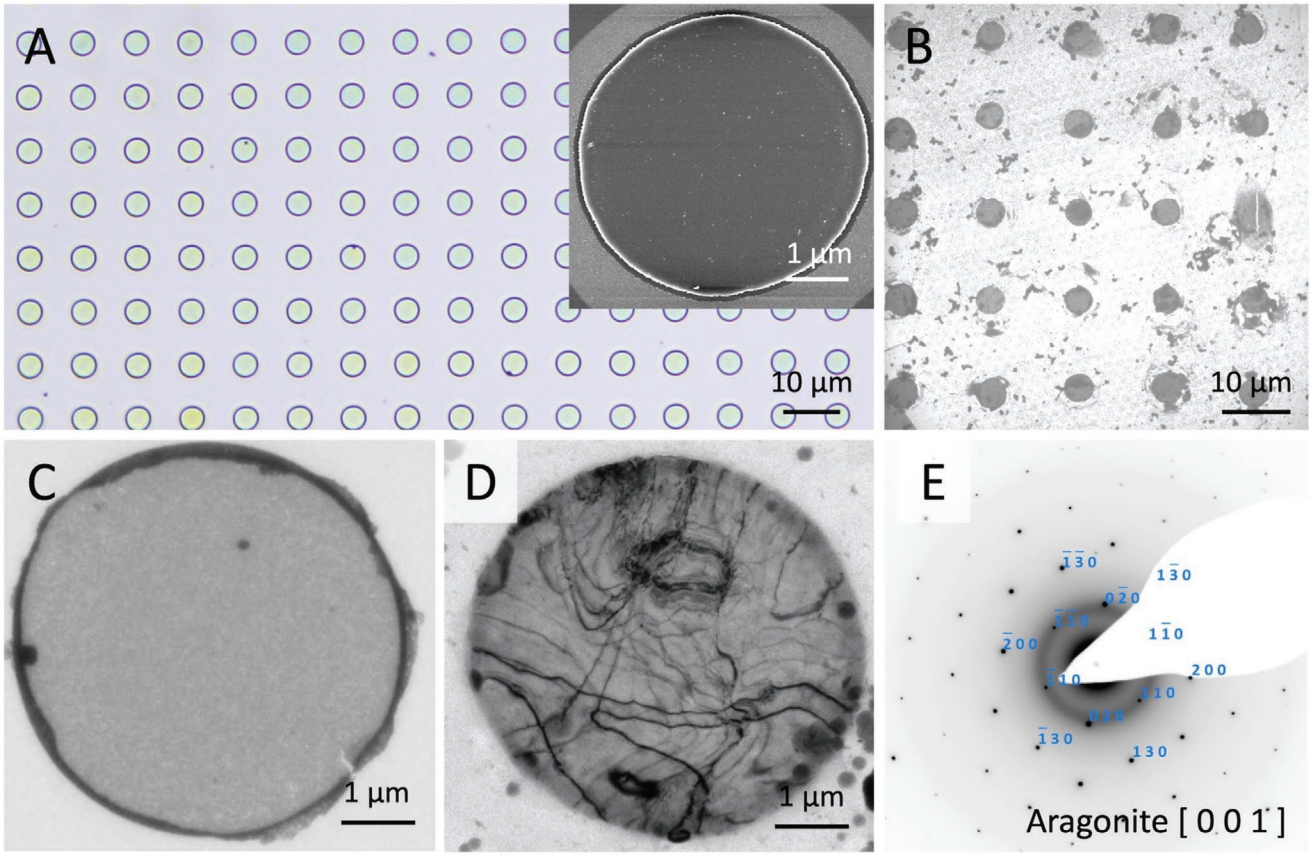

Figure 6. Patterned ACC and crystallization to aragonite. A) OM and (inset) SEM image of arrays of ACC discs with diameters of 5 µm on silicon wafers, where the ACC was produced at conditions $[Mg^{2+}] = 2 \times 10^{-3}$ M and [PAA] = 2 µg mL^{-1}. Bright-field TEM images of B) and C) ACC discs patterned on TEM grids, and D) aragonite formed on heating at 130 °C. E) SAED pattern of the aragonite single crystal shown in D).

When heated, ACC can crystallize via a true solid-state transformation, where this is accompanied by dehydration and structural rearrangements.[28,57–61] TGA analysis has shown that this can occur over a wide range of temperatures, where this is principally determined by the pH at which the ACC formed.[52,61] ACC precipitated at high pH values (pH > 12) crystallizes at ≈300–360 °C,[29,52,57,58,61–63] and temperatures of 190 °C,[61] and 160 °C[52] have been recorded for ACC precipitated around pH = 10, and 105 °C for ACC precipitated from the decomposition of dimethyl carbonate in the presence of NaOH.[64] This is attributed to the increase in hydroxyl content in the ACC at high pH values, where this occurs without any significant change in the water content.[52] The crystallization temperature also shows a dependence on particle size, and is higher for small particles,[62,65] an effect that can be correlated with their lower water contents.[65]

Both our experiments and those of others have reported higher crystallization temperatures for Mg-ACC than pure ACC in the solid-state,[19,29] and attributed them to the strong association of Mg^{2+} ions with water/hydroxyl molecules in the Mg-ACC. ACC contains two main water fractions—mobile and structural,[57,59,61] and with a few exceptions[53] Mg-ACC contains more water than pure ACC.[28,32,49] At room temperature, there is more mobile water in Mg-ACC than in pure ACC, which facilitates the molecular rearrangements that precede nucleation, making nucleation easier.[49] At elevated temperatures, in contrast, the mobile water has been lost prior to nucleation. Some structural water may remain, depending on the nucleation temperature. With just structural water present, the mobility of the ions is lower than in pure ACC, making nucleation harder.[19]

3.2. Temperature-Dependent Change of the Film Structure

Our results also demonstrate a significant change in the structures of the product films when the transformation is conducted at high temperatures as compared with ambient conditions. While conversion at room temperature yielded spherulitic structures, single crystals formed at elevated temperatures. The mechanisms by which spherulites form have been extensively discussed, where noncrystallographic branching allows spherulites to be completely space-filling.[66,67] Growth can result from secondary nucleation of crystals at the growth front, and misorientation can derive from i) impurities that induce disorder, ii) heterogeneities that form spontaneously in the surrounding medium, or iii) noncrystallographic branching at fixed misorientations.[67] A recent study of spherulitic structures in aragonite corals also suggested that nuclei may form adjacent to the growth front, and competitive growth of the anisotropic aragonite crystals then generates the spherulite.[68]

We suggest that the dramatic change in structure of the films that occurs on heating may be due to a change in the crystallization mechanism. Under ambient conditions the films crystallize via a local dissolution/ reprecipitation mechanism, and the Mg^{2+} ions, which must dehydrate prior to occlusion in the calcite lattice, disrupt growth and cause noncrystallographic branching and thus spherulite formation. At elevated temperatures, Mg-calcite nucleates and grows within a matrix of Mg-ACC that will only contain structural water at the temperatures employed. That the Mg-ACC transforms to single crystals demonstrates that the Mg^{2+} ions are less disruptive of Mg-calcite growth during a solid-state transformation of Mg-ACC than they are on growth from solution (as occurs via a dissolution/ reprecipitation mechanism). Indeed, a 0.5 × 0.5 cm Mg-ACC film that takes 2–3 days to crystallize at room temperature crystalizes with ≈5 h at T_{ON} (>100 °C).

3.3. Control Over Polymorph

The relationship between the composition of the ACC films and the polymorph of the crystalline product is particularly interesting. Magnesium was essential to the formation of aragonite, where pure aragonite only formed from ACC precipitated at $[Mg^{2+}] = 2–4 \times 10^{-3}$ M and in the absence of PAA. An increase in $[Mg^{2+}]$ to 10×10^{-3} M yielded Mg-calcite in the presence or absence of PAA. The PAA has some effect, however, where a mixture of aragonite and calcite form at $[Mg^{2+}] = 2 \times 10^{-3}$ M and [PAA] = 2 μg mL^{-1}, and magnesian calcite was the sole product at $[Mg^{2+}] = 4 \times 10^{-3}$ M and [PAA] = 4 μg mL^{-1}.

Conversion of the Mg-ACC to calcite is readily explained, where the heat-induced solid-state transformation ensures that the magnesium ions in the precursor ACC phase are preserved in the product crystals. Therefore, as aragonite can only accommodate very low levels of magnesium, all ACC samples containing over ≈1 mol% Mg convert to magnesian calcite. The influence of PAA can be attributed to the same effect, as ACC samples with higher magnesium contents are generated in its presence. That aragonite forms at lower Mg concentrations, in contrast, reveals a balance between the nucleation and growth rates of aragonite and low Mg-calcite in this composition regime that ultimately favors aragonite. Indeed, studies of aragonite and Mg-calcite precipitation in bulk solutions with different Mg/Ca ratios, pH levels, temperatures, carbonate sources, and concentrations, have shown that polymorph selection is a complex process underpinned by both kinetic and thermodynamic factors,[23,24,26,27,69] and that aragonite can be formed at both high Mg/Ca ratios and values closer to one depending on the supersaturation and carbonate concentration.[16]

That aragonite only forms within a narrow range of compositions may also explain why there are few previous examples of pseudomorphic conversions of ACC to aragonite.[11,70] The presence of low levels of Mg^{2+} ions (1–2 mol%) within ACC is clearly sufficient to inhibit the formation of calcite at 130 °C such that aragonite forms. As calcite inhibition will only increase with increasing magnesium, the change in polymorph to Mg-calcite demonstrates that aragonite formation is also inhibited at higher Mg levels in this solid-state environment. As aragonite can only accommodate very low levels of magnesium, any aragonite nuclei that form and start to grow within the Mg-ACC matrix will locally deplete calcium and carbonate ions. This will increase the Mg/Ca ratio in the vicinity of the crystal, ultimately making it impossible for aragonite to grow further.

Mg-substituted monohydrocalcite is a common intermediary phase during the transformation of Mg-ACC in solution,[18,32,45,50,51] but was not observed here as heating causes the amorphous phase to undergo significant dehydration prior

to crystallization. Interestingly, the highest Mg-ACC generated here transformed to dolomite, where the product films comprised 10–100 μm single crystal domains. Dolomite is typically synthesized either by conversion of a solid calcium carbonate precursor or a direct precipitation route.[71,72] Both methods are extremely slow at <100 °C, such that dolomite is usually synthesized under hydrothermal conditions. However, proto-dolomite (with the correct composition but not the ordered structure of dolomite) is formed from high Mg-ACC at low temperatures,[72,73] and slowly converts to dolomite with further hydrothermal heating at > 100 °C.[72] Our experiments are therefore consistent with previous work, where high Mg-ACC was converted to dolomite in ≈1 h at temperatures > 400 °C.

4. Conclusions

Our results show that crystalline calcium carbonate thin films with defined structures and compositions can be generated by the solid-state transformation of ACC containing magnesium ions and small amounts of organic additives. Using annealing to drive a pseudomorphic transformation, we generate mosaics of single crystals, whose compositions can be tuned from low magnesian calcite, to aragonite, to high magnesian calcites and finally dolomite. The formation of aragonite films is particularly interesting, where the pseudomorphic transformation of ACC to aragonite is well-recognized in biological systems,[9,10] but has seldom been achieved in synthetic systems.[11,25] While organisms achieve this by confining the ACC, such that it is isolated from bulk solution, it is difficult to create analogous confined systems synthetically. These results therefore show that the magnesium content of the ACC is critical in determining the polymorph of the crystals produced via a solid-state transformation. It would be interesting to compare the Mg contents of transient biogenic ACC samples that transform to calcite and aragonite to determine whether this strategy is also exploited in biomineralization.

5. Experimental Section

Materials: Analytical grade $(NH_4)_2CO_3$, $CaCl_2{\cdot}2H_2O$, $MgCl_2{\cdot}6H_2O$, and polyacrylic acid sodium salt (M_W 8k, 45 wt%) were purchased from Sigma-Aldrich and used as received. Deionized Milli-Q water (18.2 MΩ cm) was used for the preparation of solutions. Polydimethylsiloxane (PDMS) was prepared using a SYLGARD 184 silicon elastomer kit.

Preparation of Substrates: Silicon <100> wafers (Inseto limited) were the principal substrates used for the deposition of ACC films. These were cut into pieces of size 0.5 × 0.5 cm^2, and were cleaned thoroughly with Milli-Q deionized water and ethanol, and dried with N_2 gas. The surfaces of these substrates were then rendered hydrophilic by treating them with air plasma for 15 s prior to the precipitation experiments.

Preparation of PDMS Reaction Wells: A glass master was made by gluing a 0.5 × 0.5 cm^2 × 1 mm glass slide to a 2 × 2 cm^2 glass slide. The degassed PDMS precursor mixture (10:1 base to catalyst) was poured over the glass master, cured in a ventilated oven at 60 °C for 120 min, and then peeled off from the glass master to create the PDMS precipitation wells. For the preparation of gas permeable PDMS films, 1 mL degassed PDMS precursor liquid was spin-coated onto glass at 1000 rpm for 20 s using a Chemat spin-coater (KW-4A), and was then cured at 60 °C for 120 min.

Deposition of Amorphous Calcium Carbonate (ACC) Thin Films: ACC films were precipitated using the ammonium diffusion method (ADM)[30] from reaction solutions of composition 10×10^{-3} M $CaCl_2$, $0–100 \times 10^{-3}$ M $MgCl_2$, and 0–20 μg mL^{-1} poly(acrylic acid) (PAA) (Table 1). The solutions were filtered through 0.45 μm Isopore GTTP membrane filters (Millipore) prior to use. The process was carried out in 1 mm deep PDMS reaction wells, where silicon substrates were placed at the base of the wells, which were then covered with a gas permeable PDMS thin film (thickness = 20 μm). The precipitation solution was injected into the cell using a syringe and the cell was placed in a sealed Petri dish containing 2 g of $(NH_4)_2CO_3$ powder. The reaction was allowed to proceed from 20 min to 2 h and the substrates were then washed with ethanol and dried under a flow of N_2 gas (Table S1, Supporting Information).

Formation of ACC Micropatterns: Micropatterned substrates were prepared using standard photolithography techniques. A dark-field photomask comprising a square array of microcircles with diameters of 5–20 μm and center-to-center separations of 10 μm was purchased from Microlitho LTD. A silicon substrate that had been prior cleaned with iso-propanol was spin-coated with 0.5 mL positive photoresist (MICROPOSIT S1813) at 500 rpm for 5 s, followed by 4000 rpm for 30 s, and then soft-baked at 115 °C for 60 s. The photoresist side of the substrate was then placed in contact with the photomask and exposed to UV light using a mask aligner (KARL SUSS, MJB 3, 350–450 nm) for 5 s. The substrate was then immersed in a developer solution (MICROPOSIT MF-319) for 60 s to remove the crosslinked photoresist, and was then rinsed with copious amounts of DI water and dried with N_2 gas. ACC was then precipitated on the micropatterned substrates using the same procedure employed for the uniform substrates, followed by a lift-off of photoresist in ethanol for 10 min.

Crystallization of ACC Films: The prepared ACC films were allowed to crystallize in air by either holding them at room temperature or heating them. Heating was carried out by placing the substrates supporting the ACC films on a customized heating stage with tunable temperatures up to 300 °C and increasing the temperature by 10 °C min^{-1}. A hotplate was used for incubation above 300 °C. The crystallization process was monitored using a polarized optical microscope (Zeiss AXIO Scope A1) under reflection to identify the temperature at which crystallization started. This was termed the onset nucleation temperature (T_{ON}) and the film was then incubated at T_{ON} until crystallization was completed.

Characterization of Calcium Carbonate Thin Films: Both amorphous and crystalline calcium carbonate films were characterized using a series of techniques to determine their structures and compositions. ICP-OES was used to determine the Mg-content of the precursor ACC films, where samples were prepared by immersing 10 substrates supporting the ACC films in 1 vol% HCl for 5 min. The analysis was conducted using a Thermo Fisher Scientific iCAP 7400 radial ICP-OES Analyzer.

The thickness of ACC and calcite films were characterized with AFM using a Bruker Multimode 8 with a Nanoscope V controller. Samples of ACC films were scratched, and AFM analyses were conducted at the scratches interfaces with contact mode using silicon nitride cantilevers (model SNL-10, Bruker). The crystalline structures of the product films were characterized using polarized optical microscopy (Nikon Eclipse LV100 and Zeiss AXIO Scope A1), while the morphologies of the ACC and crystalline films were determined using scanning electron microscopy (SEM). This was conducted using a FEI NanoSEM Nova 450 at 3 kV and substrates were mounted on aluminum stubs with double sided Cu tape, and were coated with a 2 nm layer of Ir prior to analysis.

The crystalline structures of the films were investigated in detail using TEM, where samples were prepared by depositing the ACC films on TEM grids supporting SiN membranes (NanoBasic, NG01-011A, Dune sciences) that had been treated with an air plasma prior to ACC precipitation. The ACC films were then crystallized by heating the TEM grid supporting the ACC films at T_{ON}. Identical crystallization behaviors and onset temperatures were observed for both the silicon wafer and SiN/TEM substrates. The samples were examined at 200 kV using a FEI Tecnai TF20 FEG-TEM, and diffraction patterns were obtained using SAED techniques with apertures of 1 or 5 μm projected diameters. Elemental analyses of Ca^{2+} and Mg^{2+} ions in ACC and calcite films were

carried out using a high-angle annular dark field scanning transmission electron microscopy (HAADF-STEM) and energy dispersive X-ray (EDX) spectroscopy, where this was conducted in a FEI Titan Themis Cubed operated at 300 kV S/TEM with HAADF/ADF/BF STEM detectors, FEI Super-X 4-detector EDX system and a Gatan OneView 4 K CMOS digital camera.

Supporting Information

Supporting Information is available from the Wiley Online Library or from the author.

Acknowledgements

This work was supported by funding from the European Research Council (ERC) under the project DYNAMIN, Grant Agreement No. 788968 (S.Z., N.K., and F.C.M.) and an EPSRC Programme Grant which funds the Crystallization in the Real World Consortium (No. EP/R018820/1, F.C.M. and Y.Y.K.). For the purpose of open access, the author has applied a CC-BY public copyright license to any Author Accepted Manuscript (AAM) version arising from this submission. The authors thank Stephen Reid for his help with the ICP-OES analyses.

Conflict of Interest

The authors declare no conflict of interest.

Data Availability Statement

The data that support the findings of this study are openly available in Research Data Leeds Repository at https://doi.org/10.5518, reference number 1103.[74]

Keywords

ACC, aragonite, dolomite, magnesian calcite

Received: February 3, 2022
Revised: February 25, 2022
Published online: March 20, 2022

[1] L. Addadi, S. Raz, S. Weiner, *Adv. Mater.* **2003**, *15*, 959.
[2] Y. Politi, T. Arad, E. Klein, S. Weiner, L. Addadi, *Science* **2004**, *306*, 1161.
[3] S. Weiner, L. Addadi, *Ann. Rev. Mater. Res.* **2011**, *41*, 21.
[4] E. Beniash, J. Aizenberg, L. Addadi, S. Weiner, *Proc. R. Soc. London, Ser. B* **1997**, *264*, 461.
[5] L. B. Gower, *Chem. Rev.* **2008**, *108*, 4551.
[6] J. D. Rodriguez-Blanco, S. Shaw, P. Bots, T. Roncal-Herrero, L. G. Benning, *J. Alloys Compd.* **2012**, *536*, S477.
[7] J. Aizenberg, G. Lambert, S. Weiner, L. Addadi, *J. Am. Chem. Soc.* **2002**, *124*, 32.
[8] S. Raz, P. C. Hamilton, F. H. Wilt, S. Weiner, L. Addadi, *Adv. Funct. Mater.* **2003**, *13*, 480.
[9] R. T. DeVol, C. Y. Sun, M. A. Marcus, S. N. Coppersmith, S. C. B. Myneni, P. Gilbert, *J. Am. Chem. Soc.* **2015**, *137*, 13325.
[10] T. Mass, A. J. Giuffre, C. Y. Sun, C. A. Stifler, M. J. Frazier, M. Neder, N. Tamura, C. V. Stan, M. A. Marcus, P. Gilbert, *Proc. Natl. Acad. Sci. USA* **2017**, *114*, E7670.
[11] F. F. Amos, D. M. Sharbaugh, D. R. Talham, L. B. Gower, M. Fricke, D. Volkmer, *Langmuir* **2007**, *23*, 1988.
[12] N. H. Munro, K. M. McGrath, *Chem. Commun.* **2012**, *48*, 4716.
[13] S. Kajiyama, T. Nishimura, T. Sakamoto, T. Kato, *Small* **2014**, *10*, 1634.
[14] X. Long, Y. Ma, L. Qi, *J. Struct. Biol.* **2014**, *185*, 1.
[15] I. Polishchuk, A. A. Bracha, L. Bloch, D. Levy, S. Kozachkevich, Y. Etinger-Geller, Y. Kauffmann, M. Burghammer, C. Giacobbe, J. Villanova, G. Hendler, C.-Y. Sun, A. J. Giuffre, M. A. Marcus, L. Kundanati, P. Zaslansky, N. M. Pugno, P. U. P. A. Gilbert, A. Katsman, B. Pokroy, *Science* **2017**, *358*, 1294.
[16] R. A. Berner, *Geochim. Cosmochim. Acta* **1975**, *39*, 489.
[17] F. Lippmann, *Sedimentary Carbonate Minerals*, Springer, Heidelberg **1973**.
[18] E. Loste, R. M. Wilson, R. Seshadri, F. C. Meldrum, *J. Cryst. Growth* **2003**, *254*, 206.
[19] M. Alberic, L. Bertinetti, Z. Y. Zou, P. Fratzl, W. Habraken, Y. Politi, *Adv. Sci.* **2018**, *5*, 1701000.
[20] F. C. Meldrum, S. T. Hyde, *J. Cryst. Growth* **2001**, *231*, 544.
[21] M. E. Kunitake, S. P. Baker, L. A. Estroff, *MRS Commun.* **2012**, *2*, 113.
[22] K. M. Towe, P. G. Malone, *Nature* **1970**, *226*, 348.
[23] D. Wang, L. M. Hamm, A. J. Giuffre, T. Echigo, J. D. Rimstidt, J. J. De Yoreo, J. Grotzinger, P. M. Dove, *Faraday Disc.* **2012**, *159*, 371.
[24] J. M. Xto, H. C. Du, C. N. Borca, E. Amstad, J. A. van Bokhove, T. Huthwelker, *Cryst. Growth Des.* **2019**, *19*, 4385.
[25] M. L. Zeng, Y. Y. Kim, C. Anduix-Canto, C. Frontera, D. Laundy, N. Kapur, H. K. Christenson, F. C. Meldrum, *Proc. Nat. Acad. Sci. USA* **2018**, *115*, 7670.
[26] J. W. Morse, Q. W. Wang, M. Y. Tsio, *Geology* **1997**, *25*, 85.
[27] J. Lee, J. W. Morse, *Geology* **2010**, *38*, 115.
[28] A. V. Radha, A. Fernandez-Martinez, Y. D. Hu, Y. S. Jun, G. A. Waychunas, A. Navrotsky, *Geochim. Cosmochim. Acta* **2012**, *90*, 83.
[29] J. Ihli, Y.-Y. Kim, E. H. Noel, F. C. Meldrum, *Adv. Funct. Mater.* **2013**, *23*, 1575.
[30] J. Ihli, P. Bots, A. Kulak, L. G. Benning, F. C. Meldrum, *Adv. Funct. Mater.* **2013**, *23*, 1965.
[31] J. K. Berg, T. Jordan, Y. Binder, H. G. Borner, D. Gebauer, *J. Am. Chem. Soc.* **2013**, *135*, 12512.
[32] C. R. Blue, A. Giuffre, S. Mergelsberg, N. Han, J. J. De Yoreo, P. M. Dove, *Geochim. Cosmochim. Acta* **2017**, *196*, 179.
[33] J. Jiang, M. R. Gao, Y. H. Qiu, S. H. Yu, *Nanoscale* **2010**, *2*, 2358.
[34] D. Wang, A. F. Wallace, J. J. De Yoreo, P. M. Dove, *Proc. Natl. Acad. Sci. USA* **2009**, *106*, 21511.
[35] J. T. Han, X. R. Xu, D. H. Kim, K. Cho, *Adv. Funct. Mater.* **2005**, *15*, 475.
[36] J. T. Han, X. R. Xu, D. H. Kim, K. W. Cho, *Chem. Mater.* **2005**, *17*, 136.
[37] E. Seknazi, S. Kozachkevich, I. Polishchuk, N. Bianco Stein, J. Villanova, J.-P. Suuronen, C. Dejoie, P. Zaslansky, A. Katsman, B. Pokroy, *Nat. Commun.* **2019**, *10*, 4559.
[38] I. E. Bolotov, V. Y. Kolosov, A. V. Kozhyn, *Phys. Status Solidi A* **1982**, *72*, 645.
[39] B. Pokroy, A. N. Fitch, F. Marin, M. Kapon, N. Adir, E. Zolotoyabko, *J. Struct. Biol.* **2006**, *155*, 96.
[40] Z. Zou, X. Yang, M. Albéric, T. Heil, Q. Wang, B. Pokroy, Y. Politi, L. Bertinetti, *Adv. Funct. Mater.* **2020**, *30*, 2000003.
[41] J. M. Gregg, D. L. Bish, S. E. Kaczmarek, H. G. Machel, *Sedimentology* **2015**, *62*, 1749.
[42] H. Steinfink, F. J. Sans, *Am. Mineral.* **1959**, *44*, 679.
[43] C. Li, G. Hong, H. Yu, L. Qi, *Chem. Mater.* **2010**, *22*, 3206.
[44] S. Sohn, Y. Xie, Y. Jung, J. Schroers, J. J. Cha, *Nat. Commun.* **2017**, *8*, 1980.
[45] J. D. Rodriguez-Blanco, S. Shaw, P. Bots, T. Roncal-Herrero, L. G. Benning, *Geochim. Cosmochim. Acta* **2014**, *127*, 204.

[46] M. M. Reddy, K. K. Wang, *J. Cryst. Growth* **1980**, *50*, 470.
[47] A. Mucci, J. W. Morse, *Geochim. Cosmochim. Acta* **1983**, *47*, 217.
[48] W. D. Bischoff, F. T. Mackenzie, F. C. Bishop, *Geochim. Cosmochim. Acta* **1987**, *51*, 1413.
[49] Z. Liu, Z. Zhang, Z. Wang, B. Jin, D. Li, J. Tao, R. Tang, J. J. De Yoreo, *Proc. Natl. Acad. Sci. USA* **2020**, *117*, 3397.
[50] F. Konrad, B. Purgstaller, F. Gallien, V. Mavromatis, P. Gane, M. Dietzel, *J. Cryst. Growth* **2018**, *498*, 381.
[51] Y. Y. Wang, Q. Z. Yao, G. T. Zhou, S. Q. Fu, *Eur. J. Mineral.* **2015**, *27*, 717.
[52] D. J. Tobler, J. D. R. Blanco, H. O. Sorensen, S. L. S. Stipp, K. Dideriksen, *Cryst. Growth Des.* **2016**, *16*, 4500.
[53] H. Du, C. Courregelongue, J. Xto, A. Bohlen, M. Steinacher, C. N. Borca, T. Huthwelker, E. Amstad, *Chem. Mater.* **2020**, *32*, 4282.
[54] F. Konrad, F. Gallien, D. E. Gerard, M. Dietzel, *Cryst. Growth Des.* **2016**, *16*, 6310.
[55] X. Xu, J. T. Han, D. H. Kim, K. Cho, *J. Phys. Chem. B* **2006**, *110*, 2764.
[56] Y. Politi, R. A. Metzler, M. Abrecht, B. Gilbert, F. H. Wilt, I. Sagi, L. Addadi, S. Weiner, P. U. P. A. Gilbert, *Proc. Natl. Acad. Sci. USA* **2008**, *105*, 17362.
[57] J. Ihli, W. C. Wong, E. H. Noel, Y.-Y. Kim, A. N. Kulak, H. K. Christenson, M. J. Duer, F. C. Meldrum, *Nat. Commun.* **2014**, *5*, 3169.
[58] N. Koga, Y. Z. Nakagoe, H. Tanaka, *Thermochim. Acta* **1998**, *318*, 239.
[59] A. V. Radha, A. Navrotsky, *Cryst. Growth Des.* **2015**, *15*, 70.
[60] G. Wolf, C. Gunther, *J. Thermal Anal. Calorim.* **2001**, *65*, 687.
[61] M. P. Schmidt, A. J. Ilott, B. L. Phillips, R. J. Reeder, *Cryst. Growth Des.* **2014**, *14*, 938.
[62] Z. Y. Zou, L. Bertinetti, Y. Politi, A. C. S. Jensen, S. Weiner, L. Addadi, P. Fratzl, W. Habraken, *Chem. Mater.* **2015**, *27*, 4237.
[63] A. V. Radha, T. Z. Forbes, C. E. Killian, P. U. P. A. Gilbert, A. Navrotsky, *Proc. Natl. Acad. Sci. USA* **2010**, *107*, 16438.
[64] M. Faatz, F. Grohn, G. Wegner, *Adv. Mater.* **2004**, *16*, 996.
[65] H. Du, M. Steinacher, C. N. Borca, T. Huthwelker, A. Murello, F. Stellacci, E. Amstad, *J. Am. Chem. Soc.* **2018**, *140*, 14289.
[66] A. G. Shtukenberg, Y. O. Punin, E. Gunn, B. Kahr, *Chem. Rev.* **2012**, *112*, 1805.
[67] L. Granasy, L. Ratkai, A. Szallas, B. Korbuly, G. I. Toth, L. Kornyei, T. Pusztai, *Metall. Mater. Trans. A* **2014**, *45A*, 1694.
[68] C. Y. Sun, L. Granasy, C. A. Stifler, T. Zaquin, R. V. Chopdekar, N. Tamura, J. C. Weaver, J. A. Y. Zhang, S. Goffredo, G. Falini, M. A. Marcus, T. Pusztai, V. Schoeppler, T. Mass, P. Gilbert, *Acta Biomater.* **2021**, *120*, 277.
[69] U. Balthasar, M. Cusack, *Geology* **2015**, *43*, 99.
[70] L. B. Mao, H. L. Gao, H. B. Yao, L. Liu, H. Colfen, G. Liu, S. M. Chen, S. K. Li, Y. X. Yan, Y. Y. Liu, S. H. Yu, *Science* **2016**, *354*, 107.
[71] E. Usdowski, *Naturwissenschaften* **1989**, *76*, 374.
[72] J. D. Rodriguez-Blanco, S. Shaw, L. G. Benning, *Am. Mineral.* **2015**, *100*, 1172.
[73] G. Montes-Hernandez, F. Renard, A. L. Auzende, N. Findling, *Cryst. Growth Des.* **2020**, *20*, 1434.
[74] S. Zhang, O. Nahi, L. Chen, Z. Aslam, N. Kapur, Y. Y. Kim, F. C. Meldrum, Magnesium Ions Direct the Solid-State Transformation of Amorphous Calcium Carbonate Thin Films to Aragonite, Magnesium-Calcite or Dolomite; Research Data Leeds Repository, **2022**, https://doi.org/10.5518/1103.